

Field Matching: an Electrostatic Paradigm to Generate and Transfer Data

Alexander Kolesov^{*1,2} Manukhov Stepan^{*1,3} Vladimir V. Palyulin¹ Alexander Korotin^{1,2}

Abstract

We propose Electrostatic Field Matching (EFM), a novel method that is suitable for both generative modeling and distribution transfer tasks. Our approach is inspired by the physics of an electrical capacitor. We place source and target distributions on the capacitor plates and assign them positive and negative charges, respectively. We then learn the electrostatic field of the capacitor using a neural network approximator. To map the distributions to each other, we start at one plate of the capacitor and move the samples along the learned electrostatic field lines until they reach the other plate. We theoretically justify that this approach provably yields the distribution transfer. In practice, we demonstrate the performance of our EFM in toy and image data experiments.

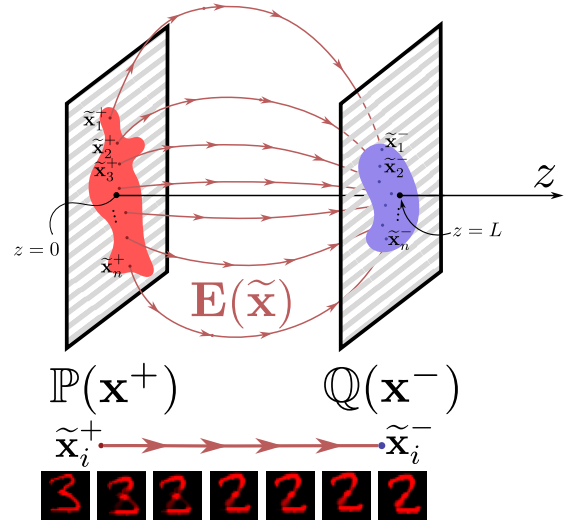


Figure 1. Our Electrostatic field matching (EFM) method. Two data distributions $\mathbb{P}(\mathbf{x}^+)$ and $\mathbb{Q}(\mathbf{x}^-)$, $\mathbf{x}^\pm \in \mathbb{R}^D$ are placed in the space \mathbb{R}^{D+1} in the planes $z = 0$ and $z = L$, respectively. The distribution $\mathbb{P}(\mathbf{x}^+)$ is assigned a positive charge, and the distribution $\mathbb{Q}(\mathbf{x}^-)$ a negative charge. These charges create an electric field $\mathbf{E}(\tilde{\mathbf{x}})$, where $\tilde{\mathbf{x}} = (\mathbf{x}, z) \in \mathbb{R}^{D+1}$. The lines of the field begin at positive charges and end at negative charges. Movement along the electric field lines provably (see our theorem 3.1) transforms the distribution $\mathbb{P}(\mathbf{x}^+)$ into the distribution $\mathbb{Q}(\mathbf{x}^-)$.

1. Introduction

The basic task of generative modeling is to learn a transformation between two distributions accessible by i.i.d. samples. The typical scenarios considered are **noise-to-data** (Goodfellow et al., 2014) and **data-to-data** (Zhu et al., 2017). These are usually referred to as the unconditional data generation and data translation, respectively.

Physics is often at the heart of the principles of generative modeling. The first attempt to link generative models and physics was made in Energy-Based models (LeCun & Huang, 2005, EBM). They parameterize data distributions using the Gibbs-Boltzmann distribution density and generate data through simulation of Langevin dynamics (Du & Mordatch, 2019; Song & Kingma, 2021).

Diffusion Models (Sohl-Dickstein et al., 2015; Ho et al., 2020; Kingma et al., 2021, DM) are a widely popular generative models' class which is inspired by *nonequilibrium thermodynamics*. The diffusion models consist of forward and

backward stochastic processes (Song et al., 2021). While the forward process corrupts the data via injection of Gaussian noise, the backward process reverses the forward process and recovers the data.

Poisson Flow Generative Models (Xu et al., 2022; 2023, PFGM) use ideas from the *electrostatic* theory for the data generation process, recovering an electric field between a hyperplane of the data and a hemisphere of large radius.

Both DM and PFGM use physical principles to corrupt data, simplifying the data distribution to a tractable one. As a result, they are only used directly for **noise-to-data** tasks.

More recently, modifications of DM have appeared that can learn diffusion in a data-to-data scenario. Diffusion Bridge Matching (Shi et al., 2024; Albergo & Vanden-Eijnden, 2023; Gushchin et al., 2024b, BM) is an SDE-based method that recovers the continuous-time Markovian process be-

^{*}Equal contribution ¹Skolkovo Institute of Science and Technology, Moscow, Russia ²Artificial Intelligence Research Institute, Moscow, Russia ³Lomonosov Moscow State University, Faculty of Physics, Moscow, Russia. Correspondence to: Alexander Kolesov <a.kolesov@skoltech.ru>.

tween data distributions. Flow matching (Lipman et al., 2023; Liu et al., 2023; Klein et al., 2024; Chen & Lipman, 2024; Xie et al., 2024, FM) is the limiting case of BM that learns ODE-based transformation between distributions.

However, there is no method based on electrostatic theory that can be applied to **data-to-data** translation tasks.

Contributions. We propose and theoretically justify a new paradigm for generative modeling called *Electrostatic Field Matching* (EFM). It is based on the electrostatic theory and suitable for both noise-to-data and data-to-data generative scenarios. We provide proof-of-concept experiments on low- and high-dimensional generative modeling tasks.

2. Background and Related Works

2.1. Basic physics

To understand the physics behind the electrostatic field matching method, let us give some basic background from standard Maxwell's 3D-electrostatics and then generalize it to the case of D dimensions. Information on Maxwell's electrostatics can be found in any electricity textbook, for instance (Landau & Lifshitz, 1971, Chapter 5).

2.1.1. MAXWELL'S ELECTROSTATICS¹

The field and the potential of a point charge. Let the point charge $q \in \mathbb{R}$ be located at the point $\mathbf{x}' \in \mathbb{R}^3$. At the point $\mathbf{x} \in \mathbb{R}^3$ it creates an electric field $\mathbf{E}(\mathbf{x}) \in \mathbb{R}^3$ equal to:

$$\mathbf{E}(\mathbf{x}) = \frac{1}{4\pi} \frac{q}{\|\mathbf{x} - \mathbf{x}'\|^3} (\mathbf{x} - \mathbf{x}'). \quad (1)$$

Note that the electric field² is a potential field, i.e., it can be expressed as a gradient of a scalar function $\varphi(\mathbf{x})$:

$$\mathbf{E}(\mathbf{x}) = -\nabla\varphi(\mathbf{x}). \quad (2)$$

The function φ is called the electric field potential. From (1), and $\nabla \frac{1}{\|\mathbf{x}\|} = -\frac{\mathbf{x}}{\|\mathbf{x}\|^3}$, we obtain that the potential of the point charge is equal:

$$\varphi(\mathbf{x}) = \frac{1}{4\pi} \frac{q}{\|\mathbf{x} - \mathbf{x}'\|}. \quad (3)$$

¹All formulas are written in the Heaviside–Lorentz system of units, where Planck's constant $\hbar = 1$, the speed of light $c = 1$, and the electric constant, which stands as a multiplier in Coulomb's law (see below), is $k = 1/(4\pi)$. This system of units is convenient for our purposes because it eliminates unnatural physical constants, and also because some formulas look particularly simple in this system of units (the Gauss's theorem and the circulation theorem).

²The meaning of electric field is as follows. If a charge q_0 is placed in an electric field, then the force acting on q_0 equals to $\mathbf{F} = q_0\mathbf{E}$. Using Eq. (1) we obtain Coulomb's law of interaction of point charges: $\mathbf{F} = k \frac{q_0 q}{\|\mathbf{x} - \mathbf{x}'\|^3} (\mathbf{x} - \mathbf{x}')$, where $k = \frac{1}{4\pi}$.

The superposition principle. If point charges q_1, q_2, \dots, q_N are located at points $\mathbf{x}_1, \mathbf{x}_2, \dots, \mathbf{x}_N$, they create independent fields $\mathbf{E}_1(\mathbf{x}), \mathbf{E}_2(\mathbf{x}), \dots, \mathbf{E}_N(\mathbf{x})$, and potentials $\varphi_1(\mathbf{x}), \varphi_2(\mathbf{x}), \dots, \varphi_N(\mathbf{x})$ at a given point $\mathbf{x} \in \mathbb{R}^3$. All these charges together create the following field and potential:

$$\begin{aligned} \mathbf{E}(\mathbf{x}) &= \sum_{n=1}^N \mathbf{E}_n(\mathbf{x}) = \sum_{n=1}^N \frac{q_n}{4\pi} \frac{(\mathbf{x} - \mathbf{x}_n)}{\|\mathbf{x} - \mathbf{x}_n\|^3}, \\ \varphi(\mathbf{x}) &= \sum_{n=1}^N \varphi_n(\mathbf{x}) = \sum_{n=1}^N \frac{1}{4\pi} \frac{q_n}{\|\mathbf{x} - \mathbf{x}_n\|}. \end{aligned} \quad (4)$$

In the general case we are dealing with a continuously distributed charge $q(\mathbf{x})$. Then the superposition principle can be written as:

$$\begin{aligned} \mathbf{E}(\mathbf{x}) &= \int \frac{1}{4\pi} \frac{(\mathbf{x} - \mathbf{x}')}{\|\mathbf{x} - \mathbf{x}'\|^3} q(\mathbf{x}') d\mathbf{x}', \\ \varphi(\mathbf{x}) &= \int \frac{1}{4\pi} \frac{1}{\|\mathbf{x} - \mathbf{x}'\|} q(\mathbf{x}') d\mathbf{x}'. \end{aligned} \quad (5)$$

Note that the charge distribution $q(\mathbf{x})$ can have values greater than zero (positive charge) or less than zero (negative charge).

An electric field strength line is a curve $\mathbf{x}(\tau) \in \mathbb{R}^3$, $\tau \in [a, b] \subset \mathbb{R}$ whose tangent to each point is parallel to the electric field at that point. In other words:

$$\frac{d\mathbf{x}(\tau)}{d\tau} = \mathbf{E}(\mathbf{x}), \text{ where } \tau \in [a, b] \subset \mathbb{R}. \quad (6)$$

The electrostatic field satisfies two theorems which define the most important properties of these lines.

Gauss's theorem (Landau & Lifshitz, 1971, §31). For any closed two-dimensional surface ∂M , which bounds the set $M \subset \mathbb{R}^3$ (see Fig. 2), the electric field flux is equal to the total charge enclosed by this surface:

$$\iint_{\partial M} \mathbf{E} \cdot d\mathbf{S} = \int_M q(\mathbf{x}) d\mathbf{x}. \quad (7)$$

In particular, it follows from Gauss's theorem that the electric field line must begin at a positive charge (or at infinity) and end at a negative charge (or at infinity). The lines cannot simply terminate in a space where there are no charges.

Theorem of electric field circulation. (Landau & Lifshitz, 1971, §26) For any closed loop ℓ (Fig. 3) the electric field circulation is equal to zero:

$$\oint_{\ell} \mathbf{E} \cdot d\mathbf{l} = 0. \quad (8)$$

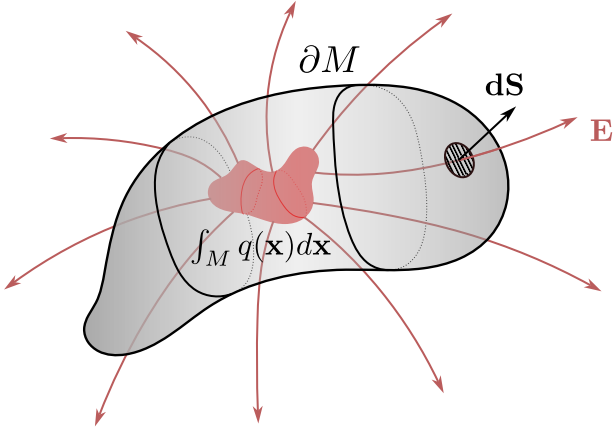


Figure 2. An illustration of the Gauss's theorem.

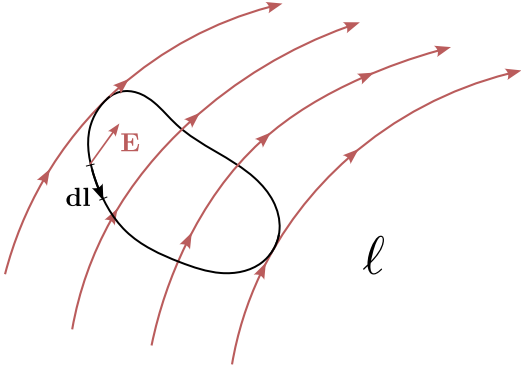


Figure 3. An illustration of the electric field circulation theorem.

It follows from the circulation theorem that there are no field lines which form closed loops.

2.1.2. D -DIMENSIONAL ELECTROSTATICS

The generalization of electrostatic equations for higher dimensions appears in discussions related to the influence of extra dimensions on the physics (Ehrenfest, 1917), (Gurevich & Mostepanenko, 1971), (Caruso et al., 2023). The generalization modifies Eqs. (7) and (8) by replacing \mathbb{R}^3 with \mathbb{R}^D and replacing dimensionality 2 of ∂M to $D - 1$ in the Gauss's theorem. The definitions in Eqs. (2), (6) and the superposition principle remain unchanged. The differences affect only the explicit expressions for the potential and the electric field.

The potential at the point $\mathbf{x} \in \mathbb{R}^D$ of a point charge q , which is located at $\mathbf{x}' \in \mathbb{R}^D$ equals to:

$$\varphi(\mathbf{x}) = \frac{1}{(D-2)S_{D-1}} \frac{q}{\|\mathbf{x} - \mathbf{x}'\|^{D-2}}, \quad (9)$$

where S_{D-1} is the surface area of an $(D-1)$ -dimensional sphere with radius 1. Then the field of the point charge is:

$$\mathbf{E}(\mathbf{x}) = -\nabla\varphi(\mathbf{x}) = \frac{q}{S_{D-1}} \frac{\mathbf{x} - \mathbf{x}'}{\|\mathbf{x} - \mathbf{x}'\|^D}. \quad (10)$$

The field of a distributed charge $q(\mathbf{x})$ can be obtained by the principle of superposition as in Eq. (5) for 3D case:

$$\mathbf{E}(\mathbf{x}) = \int \frac{1}{S_{D-1}} \frac{\mathbf{x} - \mathbf{x}'}{\|\mathbf{x} - \mathbf{x}'\|^D} q(\mathbf{x}') d\mathbf{x}'. \quad (11)$$

Together Gauss's theorem and the circulation theorem in a D -dimensional space ensure the following **principal characteristics** of electric field lines:

- (i) Electric field lines cannot terminate in points where there are no charges;
- (ii) For a system having zero total charge ($\int q(\mathbf{x}) d\mathbf{x} = 0$), electric field lines almost surely start at positive charge and end at negative charge;
- (iii) There are no electric field lines that form closed loops.

For convenience of the reader, these properties are proven in Appendix A

2.2. Poisson Flow Generative Model (PFGM)

The first attempt to couple electrostatic theory and generative modeling is proposed by (Xu et al., 2022; 2023). The authors work with a D -dimensional data distribution. They embed this distribution into $(D+1)$ -dimensional space by applying the transformation $\mathbf{x} \rightarrow \tilde{\mathbf{x}} = (\mathbf{x}, 0)$, i.e., place the data \mathbf{x} on a hyperplane $z = 0$ in $(D+1)$ -dimensional space. The data distribution is interpreted then as a positive electrostatic charge distribution.

The intuition of the method is that the charged points $\tilde{\mathbf{x}}$ in the hyperplane $z = 0$ generate the electric field $\mathbf{E}(\cdot)$ which behaves at infinity as the field of a point charge. If a point charge is placed inside a sphere S_∞ with an infinite radius, then the flux density $\mathbb{P}_\infty(\cdot)$ through the surface of the sphere is distributed uniformly. For the simplicity the authors consider the hemisphere S_∞^+ (Fig. 4b). Then:

$$\mathbb{P}_\infty(\cdot) = \mathcal{U}(S_\infty^+). \quad (12)$$

Thus, the electric field lines define the correspondence between uniformly distributed charges on the surface of the hemisphere S_∞^+ and the original data samples from $\mathbb{P}_0(\tilde{\mathbf{x}})$ in the hyperplane $z = 0$.

If a massless point charge is placed in the electric field $\mathbf{E}(\cdot)$ with field lines directed from $\mathbb{P}_0(\cdot)$ to $\mathbb{P}_\infty(\cdot)$, then the

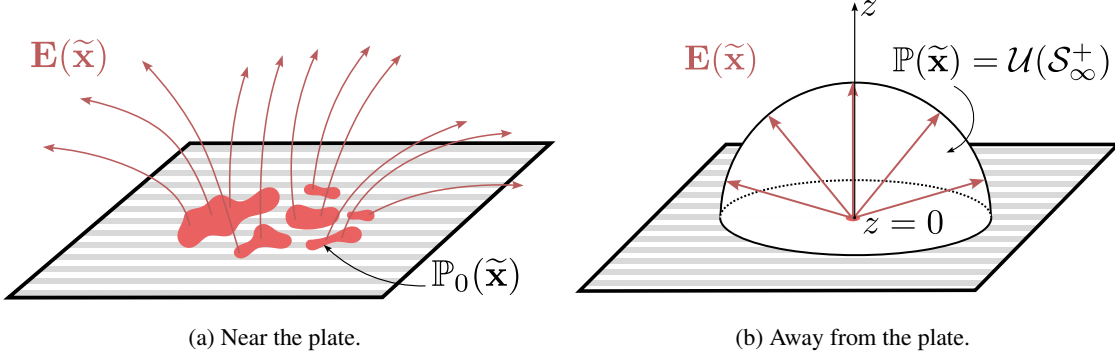


Figure 4. PFGM concept. The original data have a distribution $\mathbb{P}_0(\tilde{\mathbf{x}})$, which is assigned a positive charge that produces an electric field $\mathbf{E}(\tilde{\mathbf{x}})$. Near the plate (Fig. 4a), the field lines can have a complex structure, while away from the plate (Fig. 4b) the charge looks like a point, and therefore the electric field is uniformly distributed: $\mathbb{P}_\infty(\tilde{\mathbf{x}}) = \mathcal{U}(\mathcal{S}_\infty^+)$

charge moves along the lines to $\mathbb{P}_\infty(\cdot)$. This movement transforms the data samples from the complex distribution to the simple distribution on the hemisphere along the field lines. The corresponding inverse transformation generates the data samples from uniformly distributed samples on the hemisphere. The inverse map is a movement along these field lines in the backward direction and is defined by the following ODE with electric field $-\mathbf{E}(\cdot)$.

$$\frac{\tilde{\mathbf{x}}(t)}{dt} = -\mathbf{E}(\tilde{\mathbf{x}}). \quad (13)$$

To recover the electric field $\mathbf{E}(\cdot)$ in the extended $(D+1)$ -dimensional space, the authors propose to approximate it with a neural network $f_\theta(\cdot) : \mathbb{R}^{D+1} \rightarrow \mathbb{R}^{D+1}$.

First, they compute the ground truth electric field $\mathbf{E}(\tilde{\mathbf{x}})$ empirically at a set of arbitrary $(D+1)$ -dimensional points $\tilde{\mathbf{x}}$ inside the hemisphere \mathcal{S}_∞^+ through samples from $\mathbb{P}_0(\cdot)$ according to Eq. (11). Second, the electric field is learned at $\tilde{\mathbf{x}}$ by minimizing the difference between the predicted $f_\theta(\tilde{\mathbf{x}})$ and the ground-truth $\mathbf{E}(\tilde{\mathbf{x}})$. Having learned the electric field $\mathbf{E}(\cdot)$ in the $(D+1)$ -dimensional space, they simulate the ODE (13) with initial samples from $\mathbb{P}_\infty(\cdot)$ until the spatial coordinate z reaches 0. Finally, they get samples $\tilde{\mathbf{x}}_T \sim \mathbb{P}_0(\cdot)$, where T is the end time of the ODE simulation.

3. Electrostatic Field Matching (EFM)

This section introduces Electrostatic Field Matching (EFM), a novel generative modeling paradigm applicable to both noise-to-data and data-to-data generation grounded in electrostatic theory. The §3.1 gives an intuitive description of the method. The §3.2 gives a theoretical formulation of the method and the main theorem. In the §3.3, the learning and inference algorithms are formulated.

3.1. Intuitive explanation of the method

Our idea is to consider distributions as electric charge densities. One could assign positive charge values to the first distribution and negative charges to the second one, i.e., the charge density follows the distributions up to a sign. We then place these distributions on two D -dimensional planes at distance L from each other (Fig. 1). This will produce an electric field with lines starting at one density and finishing at another. We prove theorem 3.1 that movement along the lines allows one to make a transition from one distribution to another almost surely.

3.2. Formal theoretical justification

Let $\mathbb{P}(\mathbf{x}^+)$ and $\mathbb{Q}(\mathbf{x}^-)$, $\mathbf{x}^\pm \in \mathbb{R}^D$ be two data distributions. Let us assign to the first distribution a positive charge $q^+(\mathbf{x}^+) = \mathbb{P}(\mathbf{x}^+)$, and to the second distribution a negative charge $q^-(\mathbf{x}^-) = -\mathbb{Q}(\mathbf{x}^-)$. Note that the charge distributions are normalized to $\int q^+(\mathbf{x}^+)d\mathbf{x}^+ = 1$, $\int q^-(\mathbf{x}^-)d\mathbf{x}^- = -1$ and therefore the total charge of the system is zero.

Let us now place these distributions in $(D+1)$ -dimensional space. The new point in this space can be written as:

$$(x_1, x_2, \dots, x_D, z) = (\mathbf{x}, z) = \tilde{\mathbf{x}} \in \mathbb{R}^{D+1}. \quad (14)$$

We place $q^+(\mathbf{x}^+)$ in the hyperplane $z = 0$, and $q^-(\mathbf{x}^-)$ in the hyperplane $z = L$ (Fig. 1). One can think of it as a $(D+1)$ -dimensional **capacitor**. The distributions would be written as:

$$\begin{aligned} q^+(\tilde{\mathbf{x}}) &= q^+(\mathbf{x}, z) = q^+(\mathbf{x})\delta(z), \\ q^-(\tilde{\mathbf{x}}) &= q^-(\mathbf{x}, z) = q^-(\mathbf{x})\delta(z - L), \end{aligned} \quad (15)$$

where $\delta(\cdot)$ denotes Dirac delta function.

The electric field produced at the point $\tilde{\mathbf{x}} \in \mathbb{R}^{D+1}$ between

plates will consist of two summands:

$$\mathbf{E}(\tilde{\mathbf{x}}) = \mathbf{E}_+(\tilde{\mathbf{x}}) + \mathbf{E}_-(\tilde{\mathbf{x}}), \quad (16)$$

where $\mathbf{E}_+(\mathbf{x})$ and $\mathbf{E}_-(\tilde{\mathbf{x}})$ are the fields defined by the $q^+(\tilde{\mathbf{x}}^+)$ and $q^-(\tilde{\mathbf{x}}^-)$, respectively. The exact expression for these fields is given by Eq. (11) with replacement of D by $D+1$:

$$\mathbf{E}_\pm(\tilde{\mathbf{x}}) = \int \frac{1}{S_D} \frac{\tilde{\mathbf{x}} - \tilde{\mathbf{x}}'}{\|\tilde{\mathbf{x}} - \tilde{\mathbf{x}}'\|^{D+1}} q^\pm(\tilde{\mathbf{x}}') d\tilde{\mathbf{x}}'. \quad (17)$$

Finally, let us define the map between the distributions $T: \text{supp}(\mathbb{P}(\mathbf{x}^+)) \rightarrow \text{supp}(\mathbb{Q}(\mathbf{x}^-))$ using electric field lines. Consider a point $\tilde{\mathbf{x}}^+ = (\mathbf{x}^+, 0)$ in the support of the first distribution. Let us denote the field line $\tilde{\mathbf{x}}(\tau)$, ($\tau \in [a, b]$) starting at this point. From the properties of electric field lines formulated in Section 2.1.2, it must end almost surely at the point $\tilde{\mathbf{x}}^- = (\mathbf{x}^-, L)$ in the support of the second distribution $q^-(\tilde{\mathbf{x}}^-)$ with negative charge. Thus, $\tilde{\mathbf{x}}(a) = (\mathbf{x}^+, 0) = \tilde{\mathbf{x}}^+$, $\tilde{\mathbf{x}}(b) = (\mathbf{x}^-, L) = \tilde{\mathbf{x}}^-$. Using this, we define $T(\mathbf{x}^+) = \mathbf{x}^-$.

Then, for this map we prove the following theorem:

Theorem 3.1 (Electrostatic Field Matching). *Let \mathbf{x}^+ is distributed over $\mathbb{P}(\mathbf{x}^+)$. Then $\mathbf{x}^- = T(\mathbf{x}^+)$ is distributed over $\mathbb{Q}(\mathbf{x}^-)$ almost surely:*

$$\text{If } \mathbf{x}^+ \sim \mathbb{P}(\mathbf{x}^+) \Rightarrow T(\mathbf{x}^+) = \mathbf{x}^- \sim \mathbb{Q}(\mathbf{x}^-). \quad (18)$$

In other words, the map T defined by electric field lines does transfer $\mathbb{P}(\mathbf{x}^+)$ into $\mathbb{Q}(\mathbf{x}^-)$ indeed, as we had intended.

The proof of the theorem is given in Appendix B.

3.3. Learning and Inference Algorithm

We consider samples $\mathbf{X}^+ = \{\mathbf{x}_1^+, \dots, \mathbf{x}_N^+\}$ and $\mathbf{X}^- = \{\mathbf{x}_1^-, \dots, \mathbf{x}_M^-\}$ distributed by $\mathbb{P}(\mathbf{x}^+)$ and $\mathbb{Q}(\mathbf{x}^-)$, respectively. We then extend the space to $(D+1)$ by placing the first sample at $z=0$ and the second sample at $z=L$. Thus $\mathbf{X}^+ \rightarrow \tilde{\mathbf{X}}^+ = \{(\mathbf{x}_1^+, 0), \dots, (\mathbf{x}_N^+, 0)\} = \{\tilde{\mathbf{x}}_1^+, \dots, \tilde{\mathbf{x}}_N^+\}$ and $\mathbf{X}^- \rightarrow \tilde{\mathbf{X}}^- = \{(\mathbf{x}_1^-, L), \dots, (\mathbf{x}_M^-, L)\} = \{\tilde{\mathbf{x}}_1^-, \dots, \tilde{\mathbf{x}}_M^-\}$

Training. To recover the electric field $\mathbf{E}(\cdot)$ in $(D+1)$ -dimensional points between the hyperplanes, we approximate it with a neural network $f_\theta(\cdot): \mathbb{R}^{D+1} \rightarrow \mathbb{R}^{D+1}$. We sample the value t from the uniform distribution $\mathcal{U}(0, L)$ and take two random samples $\tilde{\mathbf{x}}^+$ and $\tilde{\mathbf{x}}^-$. Then, we get a new point $\tilde{\mathbf{x}}$ between the planes as follows:

$$\tilde{\mathbf{x}} = t\tilde{\mathbf{x}}^+ + (1-t)\tilde{\mathbf{x}}^- + \tilde{\epsilon}, \quad (19)$$

where random $\tilde{\epsilon}$ is sampled by using the following scheme. Sampling the noise ϵ from $\mathcal{N}(0, \sigma^2 I_{D+1 \times D+1})$ and calculating the Euclidean norm $\|\epsilon\|_2$, we multiply this norm by a unit Gaussian vector and get $\tilde{\epsilon}$:

$$\tilde{\epsilon} = \|\epsilon\|_2 \frac{m}{\|m\|_2}, \quad m \sim \mathcal{N}(0, I_{D+1 \times D+1}). \quad (20)$$

The ground-truth $\mathbf{E}(\tilde{\mathbf{x}})$ is estimated with Eq. (16). Specifically, the integral is approximated via Monte Carlo sampling of Eq. (11) by using samples from $\mathbb{P}(\mathbf{x}^+)$ and $\mathbb{Q}(\mathbf{x}^-)$. Then we use a neural network approximation $f_\theta(\tilde{\mathbf{x}})$ to learn the ground-truth electric field $\mathbf{E}(\tilde{\mathbf{x}})$ at points from the extended $(D+1)$ -dimensional space. We learn $f_\theta(\cdot)$ by minimising the squared error difference between the ground truth $\mathbf{E}(\tilde{\mathbf{x}})$ and the predictions $f_\theta(\tilde{\mathbf{x}})$ over the parameters of the neural network with SGD, i.e., the learning objective is

$$\mathbb{E}_{\tilde{\mathbf{x}}} \|f_\theta(\tilde{\mathbf{x}}) - \mathbf{E}(\tilde{\mathbf{x}})\|_2^2 \rightarrow \min_{\theta}. \quad (21)$$

Inference. Having learned the vector field $\mathbf{E}(\cdot)$ in the extended space with $f_\theta(\cdot)$, we simulate the movement between hyperplanes to transfer data from $\mathbb{P}(\mathbf{x}^+)$ to $\mathbb{Q}(\mathbf{x}^-)$. For this, we run an ODE solver for Eq. (13).

One needs a right stopping time for the ODE solver. In order to find it, we follow the idea of (Xu et al., 2022) and use an equivalent ODE solver with $\tilde{\mathbf{x}}$ evolving with the extended variable z :

$$d\tilde{\mathbf{x}} = d(\mathbf{x}, z) = \left(\frac{d\mathbf{x}}{dt} \frac{dt}{dz} dz, dz \right) = (\mathbf{E}_x(\tilde{\mathbf{x}}) \mathbf{E}_z^{-1}(\tilde{\mathbf{x}}), 1) dz, \quad (22)$$

where we denote $\mathbf{E}(\tilde{\mathbf{x}}) = (\mathbf{E}_x(\tilde{\mathbf{x}}), \mathbf{E}_z(\tilde{\mathbf{x}}))$. In the new ODE (22), we replace the time variable t with the physically meaningful variable z , allowing explicit start ($z=0$) and end ($z=L$) conditions. We start with samples from $\mathbb{Q}(\mathbf{x}^-)$, i.e., when $z=L$. Then, we arrive at the data distribution $\mathbb{P}(\mathbf{x}^+)$ when z reaches 0 during the ODE simulation.

All the ingredients for training and inference in our method are described in Algorithm 1, where we summarize the learning and inference procedures.

Algorithm 1 Electrostatic field matching

Input: Distributions accessible by samples:

$$\begin{aligned} &\mathbb{P}(\mathbf{x}^+) \delta(z) \text{ and } \mathbb{Q}(\mathbf{x}^-) \delta(z-L); \\ &\text{NN approximator } f_\theta(\cdot): \mathbb{R}^{D+1} \rightarrow \mathbb{R}^{D+1}; \end{aligned}$$

Repeat until converged :

$$\begin{aligned} &\text{Sample batch } \tilde{\mathbf{x}}^+ \sim \mathbb{P}(\mathbf{x}^+) \delta(z); \\ &\text{Sample batch } \tilde{\mathbf{x}}^- \sim \mathbb{Q}(\mathbf{x}^-) \delta(z-L); \\ &\text{Sample } t \sim \mathcal{U}(0, L); \\ &\text{Compute noise } \tilde{\epsilon} \text{ by (20);} \\ &\text{Calculate batch } \tilde{\mathbf{x}} = t\tilde{\mathbf{x}}^+ + (1-t)\tilde{\mathbf{x}}^- + \tilde{\epsilon}; \\ &\text{Calculate } \mathbf{E}_+(\tilde{\mathbf{x}}) \text{ and } \mathbf{E}_-(\tilde{\mathbf{x}}) \text{ through (11);} \\ &\text{Calculate } \mathbf{E}(\tilde{\mathbf{x}}) \text{ with (16);} \\ &\text{Compute } \mathcal{L} = \mathbb{E}_{\tilde{\mathbf{x}}} \|f_\theta(\tilde{\mathbf{x}}) - \mathbf{E}(\tilde{\mathbf{x}})\|_2^2 \rightarrow \min_{\theta}; \\ &\text{Update } \theta \text{ by using } \frac{\partial \mathcal{L}}{\partial \theta}; \end{aligned}$$

4. Experimental Illustrations

In this section, we demonstrate the proof-of-concept experiments with our proposed EFM method. We show a 2-

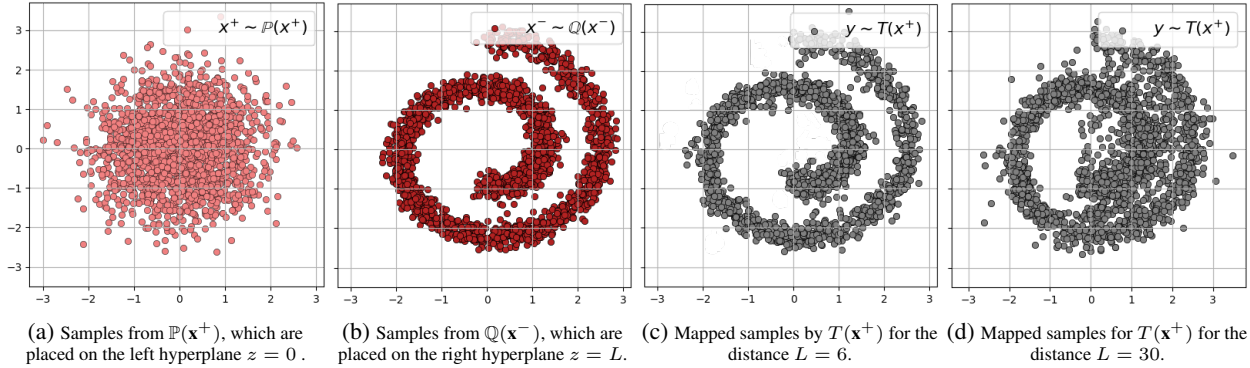


Figure 5. Illustrative 2D Gaussian \rightarrow Swiss Roll experiment: input and target distributions $\mathbb{P}(\mathbf{x}^+)$ and $\mathbb{Q}(\mathbf{x}^-)$ together with the result of the distribution transfer learned with our EFM method for distances $L = 6$ and $L = 30$ between the capacitor plates.

dimensional illustrative experiment (§4.1), image-to-image translation experiment (§4.2) and image generation experiment (§4.3) with the colored MNIST dataset. We describe details of the aforementioned experiments in Appendix C.

4.1. Gaussian to Swiss Roll Experiment

An intuitive first test to validate the method is to transfer between distributions whose densities can be visualized for comparison. We consider the 2-dimensional zero-centered Gaussian distribution with the identity covariance matrix as $\mathbb{P}(\mathbf{x}^+)$ and the Swiss Roll distribution as $\mathbb{Q}(\mathbf{x}^-)$, see their visualizations in Figs. 5a and 5b, respectively.

To show the effect of hyperparameter L in our EFM method, we do two experiments. In the first one, the samples from $\mathbb{Q}(\mathbf{x}^-)$ are placed on the hyperplane $L = 6$ (see Fig. 5c), while in the second one, we use $L = 30$ (see Fig. 5d). We show the learned trajectories of samples’ movement along the electrostatic field in Figs. 7a and 7b, respectively.

When L is small, the electric field lines are rather straight, see Fig. 7a. The learned electric field $f_\theta(\cdot) \approx \mathbf{E}(\cdot)$ allows one to accurately perform the distribution transfer, see Fig. 5c.

When the distance L between the hyperplanes is large, the learned map $T(\mathbf{x}^+)$ recovers the target density $\mathbb{Q}(\mathbf{x}^-)$ poorly (see Fig. 5d). Presumably, this is because it is more difficult to perfectly recover the electrical field $\mathbf{E}(\cdot)$ by a neural network between plates with a large distance L .

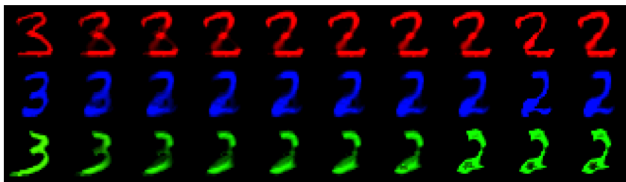


Figure 6. The sampling trajectories of our EFM method in image-to-image translation experiment, see §4.2.

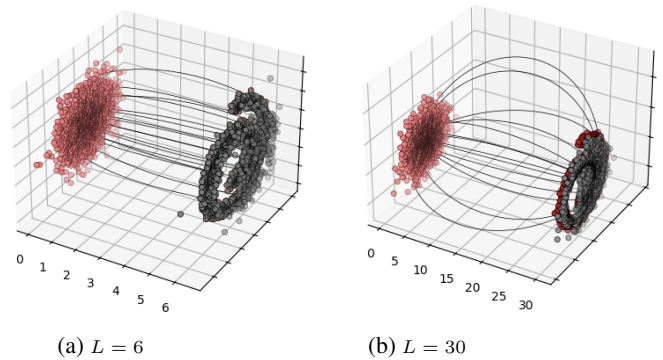


Figure 7. Electric field line structure for the Gaussian \rightarrow Swiss Roll experiment with $L = 6$ and $L = 30$. It can be seen that at large distances, the field lines are more curved than at small distances.

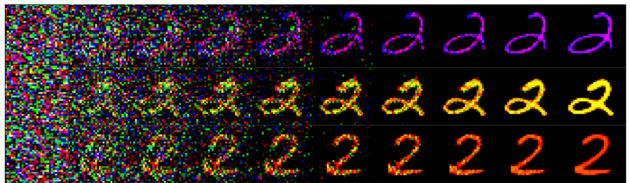


Figure 8. The Sampling trajectories of our EFM method in noise-to-image translation experiment, see §4.3.

4.2. Image-to-Image Translation Experiment

Here we consider the image-to-image translation task for transforming colored digits 3 to colored digits 2 (Gushchin et al., 2024a, §5.3). The data is based on the conventional 32×32 MNIST images dataset but the digits are randomly colored. We consider *unpaired* translation task, i.e., there is no pre-defined correspondence between digits. In other words, one colored digit 3 can be mapped to many possible digits 2 and vice versa.

We place colored digits 3 on the left hyperplane $z = 0$

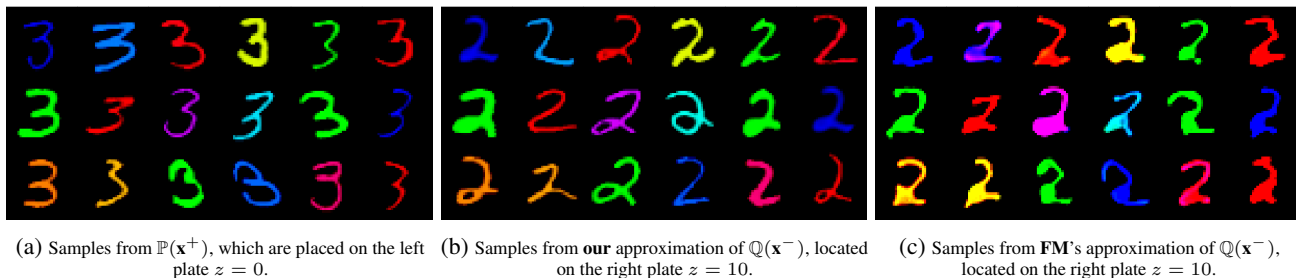


Figure 9. *Image-to-Image translation*. Pictures from the initial distribution, the result of applying our EFM method as well as the Flow Matching method are presented.

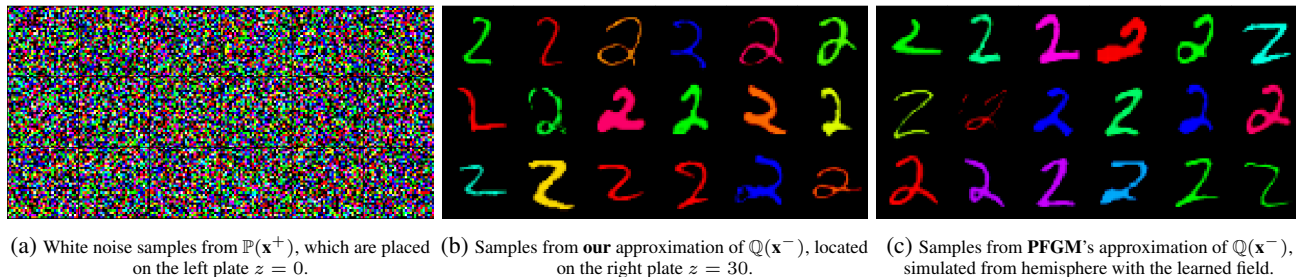


Figure 10. *Noise-to-Image generation*. Pictures from the initial distribution (Fig. 10a), the result of our EFM method (Fig. 10b) as well as the PFGM method (Fig. 10c) are presented.

and colored digits 2 on the right plate $z = 10$. We learn the electric field $\mathbf{E}(\cdot)$ between plates and show how the translation happens, see Fig. 6. For more examples of input-translated pairs, see Fig. 9.

For comparison, we add the results of the translation of the the popular ODE-based Flow Matching (FM) method (Liu et al., 2023; Lipman et al., 2023; Tong et al., 2023). The key difference between our method and FM is that FM matches to a *time*-conditional transformation (velocity), whereas our method matches to a *space*-conditional transformation (electric field). Interestingly, FM does not always accurately translate the shape and color of the initial digits 3, see Fig. 9c.

4.3. Image Generation Experiment

We also consider the task of generating 32×32 colored digits 2 from the MNIST dataset. For this task, we place white noise on the left hyperplane $z = 0$ and colored digits 2 on the right plate $z = 30$. We learn the electric field $\mathbf{E}(\cdot)$ between the plates and demonstrate recovering the distribution $\mathbb{Q}(\mathbf{x}^-)$. Also, we show the sampling trajectories for our EFM (see Fig. 8). We qualitatively see that our method recovers the target distribution $\mathbb{Q}(\mathbf{x}^-)$ of colored digits 2 (see Fig. 10b).

Also, for completeness and comparison, we show the results of generation of PFGM method which is also based on the electrostatic theory (Xu et al., 2022, PFGM), see Fig. 10c. We run the PFGM method with hyper parameters, which are described in Appendix C.

5. Discussions & Limitations

Influence of dimensionality. In high dimensions, our algorithm may require working with small numbers. Specifically, the multiplier $1/\|\mathbf{x} - \mathbf{x}'\|^D$ in the electric field formula Eq. (11) may produce values comparable to machine precision as the dimensionality of D increases. As a result, the training of our method may become less stable.

The impact of inter-plate distance L on the field estimation. The larger the inter-plate distance L is, the more curved and disperse the electric field lines become, see, e.g., Fig. 7b. Also, with an increase of this distance the electric field has to be accurately learned in a larger volume between the plates. A careful selection of the hyperparameter L may be important when applying our method.

Defining the optimal training volume. Our training approach involves sampling points $\tilde{\mathbf{x}}^+$ and $\tilde{\mathbf{x}}^-$ from the distributions, interpolating them with Eq. (19) and noising them with Eq. (20). This allows us to consider an intermediate point $\tilde{\mathbf{x}}$ between the plates (19) to learn the electrostatic field. There may exist smarter schemes to choose such points; it is a promising question of further work.

6. Impact Statement

This paper presents work whose goal is to advance the field of Machine Learning. There are many potential societal consequences of our work, none of which we feel must be specifically highlighted here.

References

- Albergo, M. and Vanden-Eijnden, E. Building normalizing flows with stochastic interpolants. In *ICLR 2023 Conference*, 2023.
- Caruso, F., Oguri, V., and Silveira, F. Still learning about space dimensionality: From the description of hydrogen atom by a generalized wave equation for dimensions $D \geq 3$. *American Journal of Physics*, 91(2):153–158, 2023.
- Chen, R. T. and Lipman, Y. Flow matching on general geometries. In *The Twelfth International Conference on Learning Representations*, 2024.
- Du, Y. and Mordatch, I. Implicit generation and modeling with energy based models. *Advances in Neural Information Processing Systems*, 32, 2019.
- Ehrenfest, P. In what way does it become manifest in the fundamental laws of physics that space has three dimensions? *Proceedings of the Amsterdam Academy of Sciences*, 20: 200–209, 1917.
- Goodfellow, I., Pouget-Abadie, J., Mirza, M., Xu, B., Warde-Farley, D., Ozair, S., Courville, A., and Bengio, Y. Generative adversarial networks. *Communications of the ACM*, 63(11):139–144, 2014.
- Gurevich, L. and Mostepanenko, V. On the existence of atoms in n-dimensional space. *Physics Letters A*, 35(3): 201–202, 1971.
- Gushchin, N., Kolesov, A., Korotin, A., Vetrov, D. P., and Burnaev, E. Entropic neural optimal transport via diffusion processes. *Advances in Neural Information Processing Systems*, 36, 2024a.
- Gushchin, N., Selikhanovych, D., Kholkin, S., Burnaev, E., and Korotin, A. Adversarial schrödinger bridge matching. In *The Thirty-eighth Annual Conference on Neural Information Processing Systems*, 2024b.
- Ho, J., Jain, A., and Abbeel, P. Denoising diffusion probabilistic models. *Advances in neural information processing systems*, 33:6840–6851, 2020.
- Kingma, D., Salimans, T., Poole, B., and Ho, J. Variational diffusion models. *Advances in neural information processing systems*, 34:21696–21707, 2021.
- Kingma, D. P. and Ba, J. L. Adam: A method for stochastic gradient descent. In *ICLR: international conference on learning representations*, pp. 1–15. ICLR US., 2015.
- Klein, L., Krämer, A., and Noé, F. Equivariant flow matching. *Advances in Neural Information Processing Systems*, 36, 2024.
- Landau, L. D. and Lifshitz, E. M. *The Classical Theory of Fields (Volume 2 of A Course of Theoretical Physics)*. Pergamon Press, 1971.
- LeCun, Y. and Huang, F. J. Loss functions for discriminative training of energy-based models. In *International workshop on artificial intelligence and statistics*, pp. 206–213. PMLR, 2005.
- Lipman, Y., Chen, R. T., Ben-Hamu, H., Nickel, M., and Le, M. Flow matching for generative modeling. In *The Eleventh International Conference on Learning Representations*, 2023.
- Liu, X., Gong, C., and qiang liu. Flow straight and fast: Learning to generate and transfer data with rectified flow. In *The Eleventh International Conference on Learning Representations*, 2023.
- Shi, Y., De Bortoli, V., Campbell, A., and Doucet, A. Diffusion schrödinger bridge matching. *Advances in Neural Information Processing Systems*, 36, 2024.
- Sohl-Dickstein, J., Weiss, E., Maheswaranathan, N., and Ganguli, S. Deep unsupervised learning using nonequilibrium thermodynamics. In *International conference on machine learning*, pp. 2256–2265. PMLR, 2015.
- Song, Y. and Kingma, D. P. How to train your energy-based models. *arXiv preprint arXiv:2101.03288*, 2021.
- Song, Y., Sohl-Dickstein, J., Kingma, D. P., Kumar, A., Ermon, S., and Poole, B. Score-based generative modeling through stochastic differential equations. In *International Conference on Learning Representations*, 2021.
- Tong, A., Malkin, N., Huguet, G., Zhang, Y., Rector-Brooks, J., Fatras, K., Wolf, G., and Bengio, Y. Conditional flow matching: Simulation-free dynamic optimal transport. *arXiv preprint arXiv:2302.00482*, 2(3), 2023.
- Xie, T., Zhu, Y., Yu, L., Yang, T., Cheng, Z., Zhang, S., Zhang, X., and Zhang, C. Reflected flow matching. *arXiv preprint arXiv:2405.16577*, 2024.
- Xu, Y., Liu, Z., Tegmark, M., and Jaakkola, T. Poisson flow generative models. In *Proceedings of the 36th International Conference on Neural Information Processing Systems*, pp. 16782–16795, 2022.
- Xu, Y., Liu, Z., Tian, Y., Tong, S., Tegmark, M., and Jaakkola, T. Pfgm++: Unlocking the potential of physics-inspired generative models. In *International Conference on Machine Learning*, pp. 38566–38591. PMLR, 2023.
- Zhu, J.-Y., Park, T., Isola, P., and Efros, A. A. Unpaired image-to-image translation using cycle-consistent adversarial networks. In *Proceedings of the IEEE international conference on computer vision*, pp. 2223–2232, 2017.

A. Properties of D -dimensional electric field lines

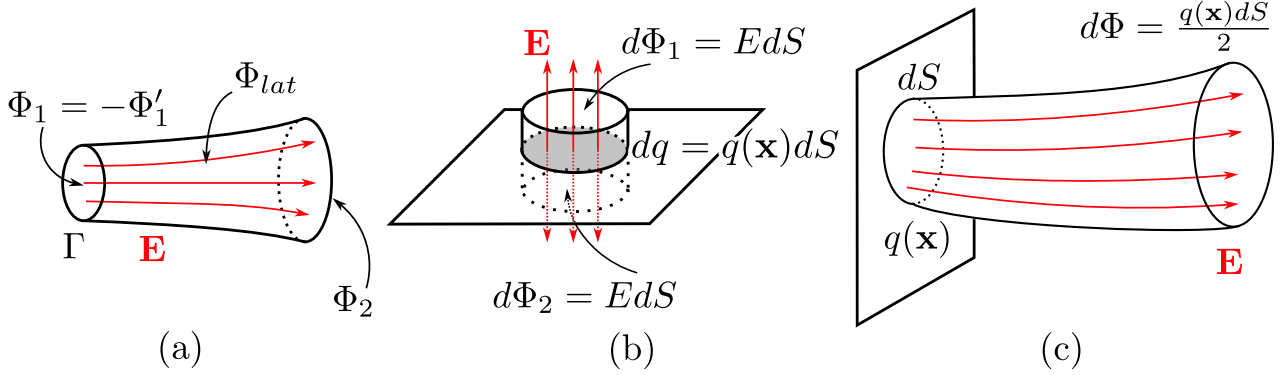


Figure 11. Electric field flux. (a) Through an arbitrary stream tube, (b) through a stream tube located infinitely close to the charged plane, (c) placed at a large distance from the charged plane.

In this Appendix the basic properties of electric field lines in D -dimensions are formulated and proved.

Definition A.1. The flux of electric field with a strength \mathbf{E} through an area $d\mathbf{S}$ is called $d\Phi = \mathbf{E} \cdot d\mathbf{S}$. The flux through a finite surface is defined as an integral:

$$\Phi = \int d\Phi = \iint \mathbf{E} \cdot d\mathbf{S}. \quad (23)$$

Definition A.2. Consider a closed piecewise smooth curve Γ placed in an electric field. A field line passes through each point of this contour. The set of these lines is called a stream surface or a stream tube (Fig.11, (a))

Lemma A.3. *The electric field flux is conserved along a stream surface if there are no charges inside that surface.*

Proof. Consider an arbitrary stream tube ∂M (Fig. 11,(a)). Note that the normal for closed surfaces is directed outwards. Near the right end of the tube, the normal and the electric field are co-directional, and near the left boundary, they have opposite directions. Therefore, $\Phi_1 = -\Phi'_1$. It is required to prove that $\Phi'_1 = \Phi_2$.

The full flux is a sum of fluxes through the ends of the tube and through its lateral surface:

$$\Phi_{full} = \Phi_1 + \Phi_2 + \Phi_{lat}. \quad (24)$$

The flux through the lateral surface, by the definition of a stream tube, must be zero: $\Phi_{lat} = 0$. Thus, $\Phi_{full} = \Phi_1 + \Phi_2 = \Phi_2 - \Phi'_1$.

From the Gauss's theorem (7):

$$\Phi_{full} = \iint_{\partial M} \mathbf{E} \cdot d\mathbf{S} = \int_M q(\mathbf{x}) d\mathbf{x} = 0. \quad (25)$$

From where it follows that $\Phi'_1 = \Phi_2$.

□

Corollary A.4. *An electric field line cannot terminate in empty space.*

Lemma A.5. *Consider a charge distribution with density $q(\mathbf{x})$ on an D -dimensional hyperplane embedded in \mathbb{R}^{D+1} . Let dS denote an element of D -dimensional surface area. For a stream tube (Fig.(11, (c)) with area dS as its base, the electric flux through this tube remains constant and is given by:*

$$d\Phi = \frac{q(\mathbf{x})dS}{2}. \quad (26)$$

Proof. Consider a stream tube in form of a cylinder and the charged surface dividing it in two equal halves. The axis of the cylinder is perpendicular to the surface. The flux through this surface will consist of three contributions: The flux through the upper base $d\Phi_1 = EdS$, the flux through the lower base $d\Phi_2 = EdS = d\Phi_1 \equiv d\Phi$, and the flux through the lateral surface $d\Phi_{lat} = 0$:

$$d\Phi_{full} = d\Phi_1 + d\Phi_2 + d\Phi_{lat} = d\Phi + d\Phi + 0 = 2d\Phi. \quad (27)$$

From the Gauss's theorem (7):

$$d\Phi_{full} = dq_{in} = q(\mathbf{x})dS. \quad (28)$$

Hence, near the surface the electric field flux is $d\Phi = \frac{1}{2}q(\mathbf{x})dS$. Since the flux is conserved along the stream tube (lemma A.3), $d\Phi = \frac{1}{2}q(\mathbf{x})dS$ at any distance from the surface, not only infinitely close to the plane.

□

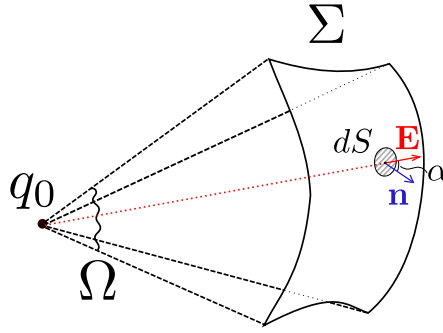


Figure 12. The field flux of a point charge q_0 through an arbitrary surface Σ seen at solid angle Ω .

Lemma A.6. Let us assume that a surface Σ can be seen at a solid angle Ω from a point charge q_0 (Fig.12). The electric field flux through this surface is equal to:

$$\Phi = \frac{q_0\Omega}{S_{D-1}}. \quad (29)$$

Proof. Divide Σ into small surface elements dS . The total flux is the integral over the entire surface, $\Phi = \int_{\Sigma} d\Phi$. By the definition of flux (A.1), and according to Eq. (10) we have:

$$d\Phi = \mathbf{E} \cdot \mathbf{dS} = EdS \cos \alpha = EdS_{\perp} = \frac{q_0}{S_{D-1}} \frac{dS_{\perp}}{r^{D-1}} = \frac{q_0 d\Omega}{S_{D-1}} \quad (30)$$

Then after integration over the solid angle, we obtain (29). □

Lemma A.7. Let there be an electrically neutral system ($\int q(\mathbf{x})d\mathbf{x} = q_+ - |q_-| = 0$) bounded in space. Then the electric field lines must begin at positive charges and end at negative charges, except perhaps for the number of lines of zero measure.

Proof. Let us assume the opposite and consider the electric field lines that start at the positive charges of the system and end at infinity (if there are no such lines, consider the lines that come from infinity and end at the negative charges). Let us denote the size of the system by $\ell = \max_{\mathbf{x}, \mathbf{y} \in \text{supp}(q)}(|\mathbf{x} - \mathbf{y}|)$. Consider moving a distance $L \gg \ell$ along these lines from the initial charge system. Let $\xi = \ell/L \ll 1$. We define the surface Σ such that it is intersected by the lines. Using the multipole decomposition of the electric field (Landau & Lifshitz, 1971, §40-41) with a first-order accuracy, we obtain:

$$\mathbf{E}|_{\Sigma} = \mathbf{E}^{(0)} + \mathbf{E}^{(1)} + \dots = \mathbf{E}_{\text{point}} + O\left(\frac{\xi}{L^{D-2}}\right), \quad (31)$$

where $\mathbf{E}^{(i)}$ is the i -th order of multipole expansion, $\mathbf{E}^{(0)} = \mathbf{E}_{\text{point}}$ is the field of a point charge. At large distance from the system the contribution of the point charge becomes the major one. All other contributions can be neglected. And therefore, in the limiting case $\xi \rightarrow 0, L \rightarrow \infty$ the formula (29) can be used. Since there is no limit on the increase of L , one can achieve an approximation accuracy as high as one needs.

Then $\Phi = \int \mathbf{E} \cdot d\mathbf{S} = (q_+ - |q_-|)\Omega/S_{D-1}(1) = 0$ by convention. Hence,

$$\int_{\Sigma} \mathbf{E} \cdot d\mathbf{S} = 0. \quad (32)$$

Therefore, if the lines that start (end) at the charges of the system and end (start) at infinity exist, their measure is zero and they do not create any flux. □

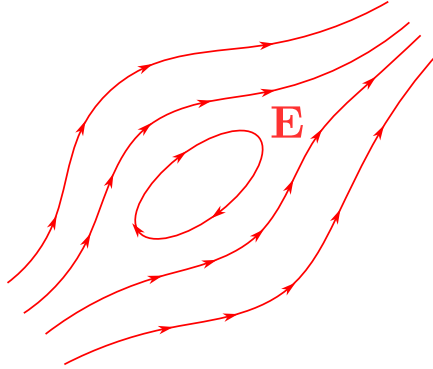


Figure 13. Closed loop of an electric field line. This situation is impossible due to the circulation theorem.

Lemma A.8. *Electric field lines cannot form closed loops (as in Fig. 13).*

Proof. Assume that there exists a closed loop ℓ along which $\oint_{\ell} \mathbf{E} \cdot d\mathbf{l} > 0$. At the same time, by virtue of the circulation theorem (8) $\oint_{\ell} \mathbf{E} \cdot d\mathbf{l} = 0$. Since the two expressions contradict to each other there can be no such thing. □

B. Proof of the Electrostatic Field Matching theorem

Theorem B.1 (Electrostatic Field Matching). *Let \mathbf{x}^+ be distributed over $\mathbb{P}(\mathbf{x}^+)$. Then $\mathbf{x}^- = T(\mathbf{x}^+)$ is distributed over $\mathbb{Q}(\mathbf{x}^-)$ almost surely:*

$$\text{If } \mathbf{x}^+ \sim \mathbb{P}(\mathbf{x}^+) \Rightarrow T(\mathbf{x}^+) = \mathbf{x}^- \sim \mathbb{Q}(\mathbf{x}^-). \quad (33)$$

Proof. Let $\{\tilde{\mathbf{x}}_i^+\}_{i=1}^n$ be a set of points distributed over the distribution $q^+(\tilde{\mathbf{x}}^+) = q^+(\mathbf{x}^+)\delta(z) = \mathbb{P}(\mathbf{x}^+)\delta(z)$. We denote the electric field lines starting at these points as $\{\tilde{\mathbf{x}}_i(\tau)\}_{i=1}^n, \tau \in [a, b] \subset \mathbb{R}$. From the properties of electric field lines (see A.7)

they must end on the support of the second distribution $q^-(\tilde{\mathbf{x}}^-) = q^-(\mathbf{x}^-)\delta(z-L) = \mathbb{Q}(\mathbf{x}^-)\delta(z-L)$, that is:

$$\frac{d\tilde{\mathbf{x}}_i}{d\tau} = \mathbf{E}(\tilde{\mathbf{x}}_i), \quad \tilde{\mathbf{x}}_i(a) = \tilde{\mathbf{x}}_i^+, \quad \tilde{\mathbf{x}}_i(b) = \tilde{\mathbf{x}}_i^-, \quad (34)$$

where $\mathbf{E}(\tilde{\mathbf{x}})$ is the field between plates (see (16)).

Let us denote by $\hat{\mathbb{Q}}_n(\tilde{\mathbf{x}}^-) = \hat{\mathbb{Q}}_n(\mathbf{x}^-)\delta(z-L)$ the effective distribution of points $\{\tilde{\mathbf{x}}_i^-\}_{i=1}^n$ from the second data set, which were obtained by moving along electric field lines. Then we have to prove that $\hat{\mathbb{Q}}_n(\mathbf{x}^-)$ converges to the true distribution $\mathbb{Q}(\mathbf{x}^-)$ with probability 1 (almost surely):

$$P\left(\lim_{n \rightarrow \infty} \hat{\mathbb{Q}}_n = \mathbb{Q}\right) = 1, \quad (35)$$

where $P(\cdot)$ is probability of a given event.

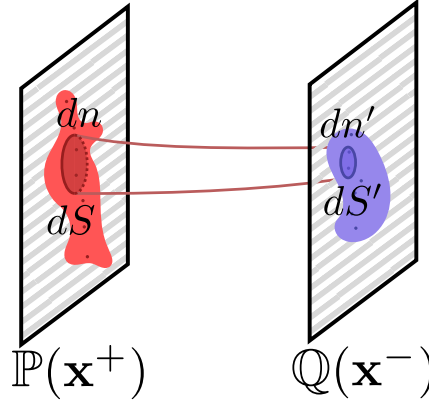


Figure 14. To the proof of the Electrostatic Field Matching theorem. Here $\mathbb{P}(\mathbf{x}^+)$ and $\mathbb{Q}(\mathbf{x}^-)$ are distributions of two sets of data. dn, dn' are the number of points $\mathbf{x}_i^+, \mathbf{x}_i^-$ that fall in the volumes dS, dS' , respectively. A stream tube starting at dS and ending at dS' is also shown.

Let us select an element of D -dimensional volume dS on the first distribution. Let dn be the number of points $\mathbf{x}_i^+ \in \mathbb{R}^D$ that are in this volume. Consider an electric field stream tube with dS as a base. Let dS' be the element of the volume into which dS has passed, and let dn' be the number of points $\mathbf{x}_i^- \in \mathbb{R}^D$ which have entered into this volume (Fig. 14).

An effective distribution $\hat{\mathbb{Q}}_n(\mathbf{x}^-)$ is:

$$\hat{\mathbb{Q}}_n(\mathbf{x}^-) = \frac{d(\text{probability})}{d(\text{volume})} = \frac{dn'}{ndS'}, \quad (36)$$

where $d(\text{probability}) = \frac{dn'}{n}$ is the probability of points \mathbf{x}_i^- falling in the $d(\text{volume}) = dS'$.

By definition, the field lines do not cross the stream tube, so $dn' = dn$.

Since the points \mathbf{x}_i^+ are distributed over $\mathbb{P}(\mathbf{x})$, due to the strong law of large numbers, the ratio dn/n converges to $\mathbb{P}(\mathbf{x})dS$ with probability one (almost surely):

$$P\left(\lim_{n \rightarrow \infty} \frac{dn}{n} = \mathbb{P}(\mathbf{x})dS\right) = 1 \iff \frac{dn}{n} \xrightarrow[n \rightarrow \infty]{\text{almost surely}} \mathbb{P}(\mathbf{x})dS \quad (37)$$

The electric field flux is conserved along the stream tube and is equal to (A.5):

$$d\Phi = \frac{\mathbb{P}(\mathbf{x}^+)dS}{2} = \frac{\mathbb{Q}(\mathbf{x}^-)dS'}{2}. \quad (38)$$

From whence we get:

$$\hat{\mathbb{Q}}_n(\mathbf{x}^+)dS' = \frac{dn'}{n} = \frac{dn}{n} \xrightarrow[n \rightarrow \infty]{\text{almost surely}} \mathbb{P}(\mathbf{x}^+)dS = \mathbb{Q}(\mathbf{x}^-)dS', \quad (39)$$

which proves the theorem. □

C. Experimental details

We aggregate the hyper-parameters of our Algorithm 1 for different experiments in the Table 1. We base our code for the experiments on PFGM’s code https://github.com/Newbeeer/Poisson_flow.

In the 2D illustrative example (see §4.1), we make the inference by constructing the ODE Euler solver for the equation 13 with the following iterative scheme:

$$\tilde{\mathbf{x}}_{t+1} = \tilde{\mathbf{x}}_t + \lambda \mathbf{E}(\tilde{\mathbf{x}}_t). \quad (40)$$

We use the learning rate $\lambda = 2e - 3$ and number of steps $NFE = 20$ to reach the right hyperplane $z = 6$.

In the case of the Image experiments (see §4.2 and §4.3), we use the RK45 ODE solver provided by <https://docs.scipy.org/doc/scipy/reference/generated/scipy.integrate.RK45.html> for the inference process with the hyper-parameters $rtol=1e-4$, $atol=1e-4$ and number of steps (NFE) equals to 100. Also, we use Exponential Moving Averaging (EMA) technique with the ema rate decay equals to 0.99. As for the optimization procedure, we use Adam optimizer (Kingma & Ba, 2015) with the learning rate $\lambda = 2e - 4$ and weight decay equals to $1e-4$.

Evaluation of the training time for our solver on the image’s experiments (see §4.2 and §4.3) takes less than 10 hours on a single GPU GTX 1080ti (11 GB VRAM).

Experiment	D	Batch Size	L	NFE , Num Steps	λ , LR	Weight Decay	σ
Gaussian Swiss-roll	2	1024	6	20	$2e-3$	0.	0.001
Colored MNIST Translation (3→2)	3072	64	10	100	$2e-4$	$1e-4$	0.01
Colored MNIST Generation	3072	64	30	100	$2e-4$	$1e-4$	0.01

Table 1. Hyper-parameters of Algorithm 1 for different experiments, where D is the dimensionality of task, L is the distance between plates and σ is used for the definition points between plates (see §3.3).

We use the source code <https://github.com/Newbeeer/pfgmpp> for running PFGM in our experiments. We found the following values of hyper parameters are appropriate for us: $\gamma = 5$, $\tau = 0.3$, $\epsilon = 1e - 3$, see (Xu et al., 2022) for details.

Also, we utilize the source code of Flow Matching (FM) from the github page <https://github.com/atong01/conditional-flow-matching/tree/main> in the experiment §4.2.